

Diffusion Dataset Condensation: Training Your Diffusion Model Faster with Less Data

Rui Huang^{1,2*} Shitong Shao^{1*} Zikai Zhou¹ Pukun Zhao¹ Hangyu Guo³
 Tian Ye¹ Lichen Bai¹ Shuo Yang³ Zeke Xie^{1†}

¹ xLeaF Lab, Hong Kong University of Science and Technology (Guangzhou)

² University of Electronic Science and Technology of China

³ Harbin Institute of Technology, Shenzhen

Abstract

Diffusion models have achieved remarkable success in various generative tasks, but training them remains highly resource-intensive, often with millions of images and GPU days of computation required. From a data-centric perspective addressing the limitation, we study diffusion dataset condensation as a new challenging problem setting that aims at constructing a “synthetic” sub-dataset with significantly fewer samples than the original dataset for training high-quality diffusion models significantly faster. To the best of our knowledge, we are the first to formally study the dataset condensation task for diffusion models, while conventional dataset condensation focused on training discriminative models. For this new challenge, we further propose a novel **Diffusion Dataset Condensation (D^2C)** framework, that consists of two phases: *Select* and *Attach*. The *Select* phase identifies a compact and diverse subset via a diffusion difficulty score and interval sampling, upon which the *Attach* phase enhances conditional signals and information of the selected subset by attaching rich semantic and visual representations. Extensive experiments across dataset sizes, model architectures, and resolutions demonstrate that our D^2C can train diffusion models significantly faster with dramatically fewer data while retaining high visual quality. Notably, for the SiT-XL/2 architecture, our D^2C achieves a $100\times$ acceleration, reaching a FID of 4.3 in just 40k steps using only 0.8% of the training data.

1 Introduction

Generative models, such as score-based [1–4] and flow-based [5–7] approaches, have achieved remarkable success in various generative tasks, producing high-quality and diverse data across domains [8–10]. However, these approaches are notoriously data and compute intensive to train, often requiring millions of samples and hundreds of thousands of iterations to capture complex high-dimensional distributions [11–13]. The resulting cost presents a significant barrier to broader application and iteration within the AIGC community, making efficient training increasingly important across both academic and industrial settings [14, 15]. Recent efforts have improved diffusion training efficiency through various strategies, such as architectural redesigns [13, 16, 11], attention optimization [17], reweighting strategies [18–20, 8], and representation learning [12]. In parallel, data-centric approaches such as Patch Diffusion [21] and advanced augmentation techniques [8] aim to better exploit the potential of existing data. Despite these advancements, the exploration of building a relatively complete “synthetic” subset through dataset condensation [22] to accelerate diffusion model training with minimal information loss remains underexplored.

* Equal contribution.

† Correspondence to zekexie@hkust-gz.edu.cn.

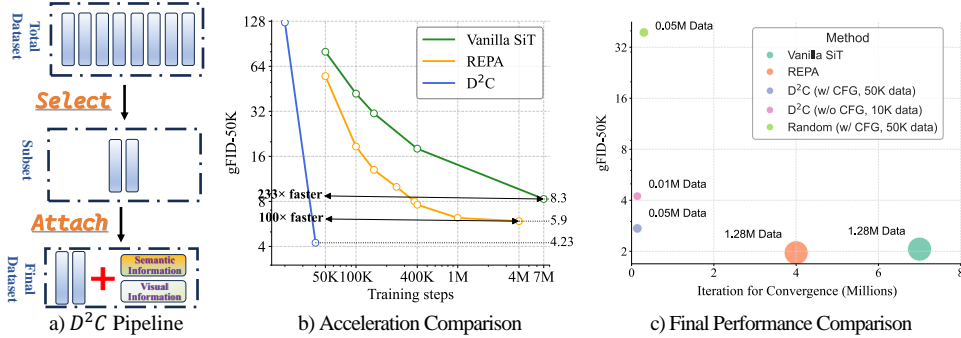


Figure 1: **Our D^2C framework significantly accelerates diffusion model training with limited data.** (a) Overview of our D^2C pipeline, which consists of a *Select* phase that filters a compact and diverse subset via diffusion difficulty score and interval sampling, and an *Attach* phase that enriches samples with semantic and visual information. (b) D^2C achieves over $100\times$ faster convergence compared to REPA and over $233\times$ faster than vanilla SiT-XL/2, reaching a FID of 4.3 at just 40k steps. (c) Under a strict 4% data budget (0.05M), our method achieves a FID of 2.7 at 180k iterations, demonstrating its strong training efficiency and rapid convergence.

Dataset condensation [22–25] aims to construct a “synthetic” sub-dataset with significantly fewer samples than the original dataset, such that a model trained from scratch on this subset achieves comparable performance to one trained on the full dataset. Unlike data pruning or selection [26], which passively select existing samples, condensation actively optimizes synthetic data, offering greater potential for aggressive data reduction and training efficiency [27]. However, all existing methods are designed for discriminative tasks. Compared to discriminative tasks, generative tasks are much more complex and demand higher dataset quality [28]. Applying popular methods (e.g., SRe²L [24]) that have substantiated effective for discriminative tasks to diffusion models presents significant challenges, such as the failure to produce diverse, high-quality outputs with structural and semantic fidelity, leading to degraded results and unstable convergence (see Sec. 4).

We raise a key question: “Can we train diffusion models dramatically faster with significantly less data, while retaining high generation quality?” The answer is affirmative. Answering this question holds significant relevance for the further development of visually generative intelligence and is therefore extremely worthwhile to explore. In this paper, we mainly made the following contributions.

First, to the best of our knowledge, we are the first to formally study the dataset condensation task for diffusion models, a new challenging problem setting that aims at constructing a “synthetic” sub-dataset with significantly fewer samples than the original dataset for training high-quality diffusion models significantly faster. More specifically, our explorations with the diffusion model provide the first insights into the challenges and potential solutions for applying dataset condensation to vision generation tasks. We note that while conventional dataset condensation made great progress and sometimes use diffusion models to construct a subset, this line of research only focused on training discriminative models instead of generative models.

Second, we propose a novel two-stage **Diffusion Dataset Condensation (D^2C)** framework, consisting of *Select* and *Attach*, illustrated in Fig. 1 (a). Our framework addresses the challenges of dataset condensation for diffusion models by decomposing the problem into two key aspects: the *Select* stage identifies an informative, compact, and learnable subset by ranking samples using the diffusion difficulty score derived from a pre-trained diffusion model; the *Attach* stage enriches each selected sample by adding semantic and visual representations, further enhancing the training efficiency while preserving performance.

Third, extensive experiments demonstrate that the proposed D^2C can train diffusion models significantly faster with dramatically fewer data while retaining high visual quality, substantiating the effectiveness and scalability. Specifically, D^2C significantly outperforms random sampling and several popular dataset selection and distillation algorithms (e.g., SRe²L [24] and K-Center) across data compression ratios of 0.8%, 4%, and 8%, at resolutions of 256×256 and 512×512 , and with both SiT [13] and DiT [11] architectures. In particular, D^2C achieves a FID of 4.3 in merely 40k training steps (w/o classifier-free guidance (CFG) [4]) using SiT-XL/2 [13], demonstrating a $100\times$

acceleration over REPA [12] and a $233\times$ speed-up compared to vanilla SiT. Furthermore, it further improves to a FID of 2.7 using only 50k synthesized images with CFG (refer to Fig. 1 (c)).

2 Preliminaries and Related Work

In this section, we briefly review diffusion models as well as dataset condensation.

Diffusion Models. We briefly introduce the standard latent-space noise injection formulation that underlies many diffusion models [6, 11, 9]. These models define a forward process that gradually perturbs input data with Gaussian noise, and train a neural network to approximate the reverse denoising process for sampling (see Appendix B for more details).

Let the original variable be denoted as $\mathbf{x}_0 \sim q_0(\mathbf{x})$. The forward diffusion process is typically implemented as a Markov chain with Gaussian noise injections:

$$q_t(\mathbf{x}_t | \mathbf{x}_0) = \mathcal{N}(\mathbf{x}_t; \alpha_t \mathbf{x}_0, \sigma_t^2 \mathbf{I}), \quad (1)$$

where $\alpha_t, \sigma_t \in \mathbb{R}^+$ are differentiable functions of t with bounded derivatives. The choice for α_t and σ_t is referred to as the noise schedule of a diffusion model. A commonly used reparameterization in score-based diffusion models [3] expresses the noisy data \mathbf{x}_t at time step t as $\mathbf{x}_t = \alpha_t \mathbf{x}_0 + \sigma_t \epsilon$, where $\epsilon \sim \mathcal{N}(0, \mathbf{I})$. In this case, to recover “clean” data from noise, a neural network $\epsilon_\theta(\cdot, \cdot, \cdot)$ is trained to predict the added noise ϵ , thereby approximating the reverse process. This framework adopts the conventional noise prediction strategy for training, where the training objective is to minimize the mean squared error between the predicted and the ground true noise:

$$\mathcal{L}_{\text{diff}} = \mathbb{E}_{\mathbf{x}_0 \sim q_0(\mathbf{x}), \epsilon \sim \mathcal{N}(0, \mathbf{I}), t \sim \mathcal{U}[0, 1]} [\|\epsilon - \epsilon_\theta(\mathbf{x}_t, t, \mathbf{c})\|_2^2], \quad (2)$$

Here, \mathbf{c} is a conditional input, such as class labels or text embeddings. In some cases, the prediction target is replaced with a linear combination of noise and data (e.g. v -prediction), which corresponds to flow matching [5–7]:

$$\mathcal{L}_{\text{velocity}} = \mathbb{E}_{\mathbf{x}_0 \sim q_0(\mathbf{x}), \epsilon \sim \mathcal{N}(0, \mathbf{I}), t \sim \mathcal{U}[0, 1]} [\|\mathbf{v}_\theta(\mathbf{x}_t, t) - (\epsilon - \mathbf{x}_0)\|_2^2]. \quad (3)$$

Here, $\mathbf{v}_\theta(\mathbf{x}_t, t)$ denotes the learned time-dependent velocity field.

Data-centric Efficient Training. Various model-side strategies have been proposed to accelerate diffusion model, including architectural enhancements [17, 11, 13], sampling refinements [18–20, 8], and representation-level techniques that leverage pretrained vision features [12, 29]. However, relatively little has been explored from a data-centric perspective. In data-centric model training, given an original dataset $\mathcal{D} = (\hat{\mathbf{X}}, \hat{\mathbf{Y}}) = \{(\hat{\mathbf{x}}_i, \hat{y}_i)\}_{i=1}^{|\mathcal{D}|}$, where each \hat{y}_i is the label corresponding to sample $\hat{\mathbf{x}}_i$, dataset compression aims to reduce the size of training data while preserving model performance. Two primary strategies have been extensively studied in this context: dataset pruning and dataset condensation.

1) *Dataset Pruning.* Dataset pruning selects an information-enrichment subset from the original dataset, i.e., $\mathcal{D}^{\text{core}} \subset \mathcal{D}$ with $|\mathcal{D}^{\text{core}}| \ll |\mathcal{D}|$, and directly minimizes the training loss over the subset:

$$\min_{\theta} \mathbb{E}_{(\mathbf{x}, y) \sim \mathcal{D}^{\text{core}}} [\ell(\phi_{\theta_{\mathcal{D}^{\text{core}}}}(\mathbf{x}), y)], \quad (4)$$

where $\ell(\cdot, \cdot)$ denotes the empirical training loss, and $\phi_{\theta_{\mathcal{D}^{\text{core}}}}$ is the model parameterized by $\theta_{\mathcal{D}^{\text{core}}}$. Classical data pruning methods like random sampling, K-Center [30], and Herding [31] can be used with diffusion models, but they offer minimal performance improvements.

2) *Dataset Condensation.* In contrast, dataset condensation aims to synthesize a small, compact, and diverse synthetic dataset $\mathcal{D}^{\mathcal{S}} = (\mathbf{X}, \mathbf{Y}) = \{(\mathbf{x}_j, y_j)\}_{j=1}^{|\mathcal{D}^{\mathcal{S}}|}$ to replace the original dataset \mathcal{D} . The synthetic dataset $\mathcal{D}^{\mathcal{S}}$ is generated by a condensation algorithm \mathcal{C} such that $\mathcal{D}^{\mathcal{S}} \in \mathcal{C}(\mathcal{D})$, with $|\mathcal{D}^{\mathcal{S}}| \ll |\mathcal{D}|$. Each y_j corresponds to the synthetic label for the sample \mathbf{x}_j .

The key motivation for dataset condensation is to create $\mathcal{D}^{\mathcal{S}}$ such that models trained on it can achieve performance within an acceptable deviation η compared to models trained on \mathcal{D} . This can be formally expressed as:

$$\sup \left\{ \left| \ell(\phi_{\theta_{\mathcal{D}}}(\hat{\mathbf{x}}), \hat{y}) - \ell(\phi_{\theta_{\mathcal{D}^{\mathcal{S}}}}(\hat{\mathbf{x}}), \hat{y}) \right| \right\}_{(\hat{\mathbf{x}}, \hat{y}) \sim \mathcal{D}} \leq \eta, \quad (5)$$

where $\theta_{\mathcal{D}}$ is the parameter set of the neural network ϕ optimized on \mathcal{D} : $\theta_{\mathcal{D}} = \arg \min_{\theta} \mathbb{E}_{(\hat{\mathbf{x}}, \hat{y}) \sim \mathcal{D}} [\ell(\phi_{\theta}(\hat{\mathbf{x}}), \hat{y})]$. A similar definition applies to $\theta_{\mathcal{D}^{\mathcal{S}}}$, which is optimized on the synthetic dataset $\mathcal{D}^{\mathcal{S}}$. Existing methods, such as RDED, MTT, SRe²L, and G-VBSM [27, 24, 25, 32, 33],

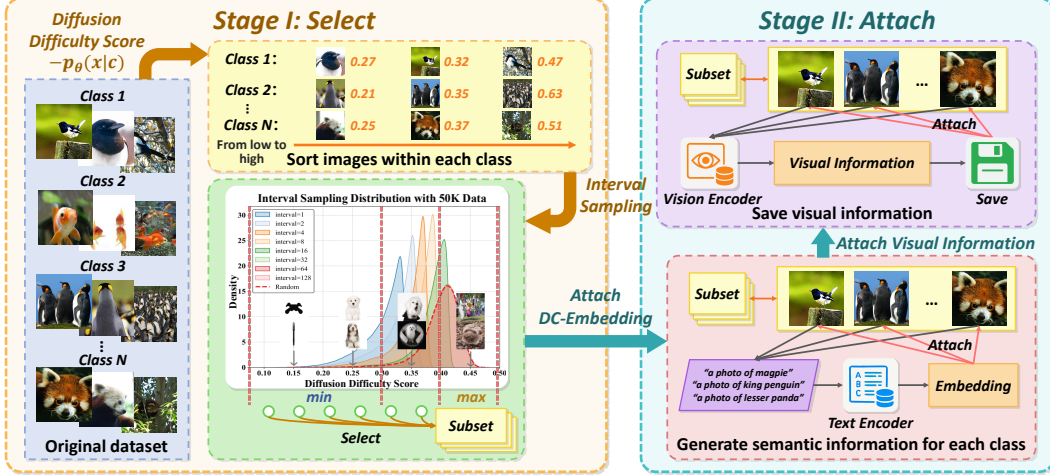


Figure 2: Overview of **Diffusion Dataset Condensation (D^2C)**. D^2C employs a two-stage process: *Select* and *Attach*. The *Select* stage identifies a compact and diverse subset by interval sampling using the diffusion difficulty score derived from a pre-trained diffusion model. The *Attach* stage further enriches each selected sample by adding semantic information and visual information.

are primarily designed for discriminative tasks. When applied to diffusion models, these methods generate synthetic images that deviate from the original data distribution, leading to detrimental effects on model training. Visualization of these synthesized images can be found at Appendix I.

3 Diffusion Dataset Condensation

To enable data-centric efficient training of diffusion models under limited resources, we propose **Diffusion Dataset Condensation (D^2C)**, the first unified framework that systematically condenses training data for diffusion models. As illustrated in Fig. 2, this process produces a condensed dataset suitable for efficient diffusion model training. D^2C consists of two stages: *Select* (Sec. 3.1), which identifies a compact set of diverse and learnable real images using *diffusion difficulty score* and *interval sampling* techniques; and *Attach* (Sec. 3.2), which augments each selected image with semantic and visual information to improve generation performance. Finally, we present the novel training paradigm utilizing the condensed dataset generated by D^2C (Sec. 3.3).

3.1 *Select*: Difficulty-Aware Selection

In this work, we focus on class-to-image (C2I) synthesis. Given a class-conditioned dataset $\mathcal{D} = \bigcup_{y=1}^C \mathcal{D}_y$, where $\mathcal{D}_y = \{x_i\}_{i=1}^{|\mathcal{D}_y|}$ denotes all samples of class y , we aim to select a compact subset for efficient diffusion training. To achieve this, we propose *diffusion difficulty score* to quantify the denoising difficulty of each sample, followed by our designed *interval sampling* to ensure diversity within the selected subset.

Diffusion Difficulty Score. The arrangement of samples from easy to hard is crucial for revealing underlying data patterns and facilitating difficulty-aware selection. Recent work [34] demonstrates that diffusion models inherently encode semantic-related class-conditional probability $p_{\theta}(c|x)$ through the variational lower bound (i.e., diffusion loss Eq. 2) of $\log p_{\theta}(x|c)$ [3, 1]. This conditional probability can be formulated as $p_{\theta}(c|x) = \frac{p_{\theta}(x|c)p(c)}{\sum_{\hat{c}} p_{\theta}(x|\hat{c})p(\hat{c})}$. Intuitively, a larger $p_{\theta}(c|x)$ indicates that sample x can be more confidently identified as belonging to class c , thus suggesting lower learning difficulty. Given the significant computational overhead of the full Bayesian formulation and our focus on estimating sample difficulty, we ignore the denominator part $\sum_{\hat{c}} p_{\theta}(x|\hat{c})p(\hat{c})$ of the calculation. Since the category $y \sim U\{0, \dots, C\}$ (C denotes the class number) is obtained by uniform sampling, and assuming $\sup\{|\mathbb{E}_{\hat{c}}[p_{\theta}(x_1|\hat{c})] - \mathbb{E}_{\hat{c}}[p_{\theta}(x_2|\hat{c})]|\}_{x_1, x_2 \sim \mathcal{D}^x} \leq \eta$ (\mathcal{D}^x denotes the all images in the dataset), we define the diffusion difficulty score based on the class-conditional probability $p_{\theta}(x|c) \propto \frac{p_{\theta}(x|c)}{\sum_{\hat{c}} p_{\theta}(x|\hat{c})} = p_{\theta}(c|x) (\sum_{\hat{c}} p_{\theta}(x|\hat{c}))$ can be viewed as a constant when sorting

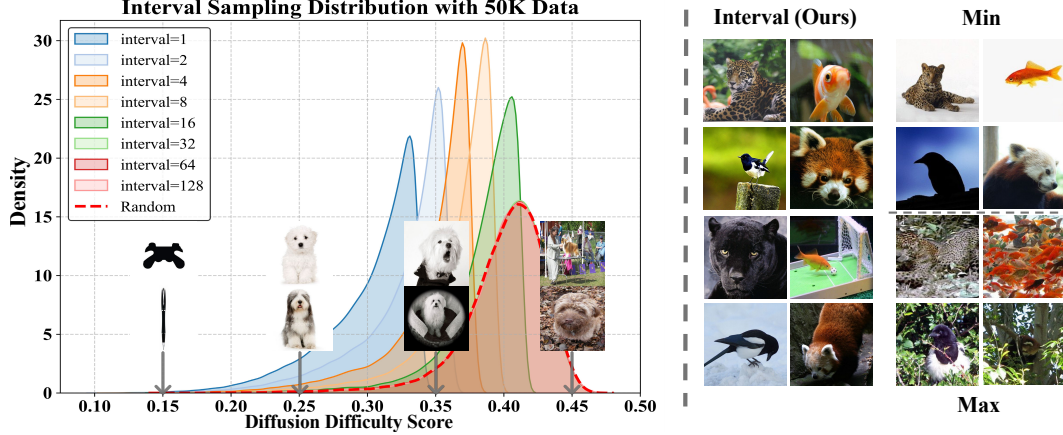


Figure 3: **Left:** Distribution of diffusion difficulty scores under different interval values k . Smaller intervals (e.g., 1, 2) favor low-loss samples, while larger intervals (e.g., 64, 128) result in a distribution closer to random sampling, thus approximating the original data distribution. Moderate intervals (e.g., 16) provide balanced coverage across difficulty levels. **Right:** Representative samples selected by three strategies: *Min* (lowest score), *Max* (highest score), and *Interval* (our proposed strategy). Interval sampling achieves a balance between structural clarity and contextual richness.

by sample difficulty):

$$s_{\text{diff}}(\mathbf{x}) = -p_{\theta}(\mathbf{x}|\mathbf{c}) = -\log \left(\exp \left(-\mathbb{E}_{\epsilon \sim \mathcal{N}(0, \mathbf{I}), t \sim \mathcal{U}[0, 1]} \left[\|\epsilon - \epsilon_{\theta}(\alpha_t \mathbf{x} + \sigma_t \epsilon, t, \mathbf{c})\|_2^2 \right] \right) \right), \quad (6)$$

The higher the score $s_{\text{diff}}(\mathbf{x})$, the easier it is, and the lower the score $s_{\text{diff}}(\mathbf{x})$, the more difficult it is. Note that in this paper’s figures and tables, we directly use the diffusion loss (i.e., $\propto -p_{\theta}(\mathbf{c}|\mathbf{x})$) for ease of understanding.

By computing $s_{\text{diff}}(x)$ for all training samples, we construct a ranked dataset. As shown in Fig. 3 (Left), these scores exhibit a skewed unimodal distribution. Selecting the easiest samples (*Min*) yields a subset dominated by clean, background-simple images with high learnability but limited diversity. In contrast, selecting only the highest-score samples (*Max*) results in cluttered, noisy, and ambiguous images that are difficult to optimize. Meanwhile, many samples lie in the middle range, offering moderate learnability but richer contextual information.

Interval Sampling. To balance diversity and learnability, we propose an *interval sampling* strategy. Specifically, we sort its images \mathcal{D}_y within each class y in ascending order of $s_{\text{diff}}(x)$ and select samples at a fixed interval k :

$$\mathcal{D}_{\text{IS}} = \bigcup_{y=1}^C \left\{ x^{(i)} \in \mathcal{D}_y \mid i \in \{0, k, 2k, \dots\} \right\}, \quad (7)$$

where \mathcal{D}_{IS} denotes the selected subset constructed by interval sampling, k is the fixed sampling interval, and $x^{(i)}$ is the i -th sample in the sorted list (e.g., $x^{(0)}$ corresponds to the sample with the lowest diffusion difficulty score). Interval sampling with a larger interval k promotes diversity in the sampled data while potentially hindering learnability. As shown in Fig. 3 (Left), this trade-off arises from a shift in the sample distribution: a larger k leads to a reduction in the number of easy samples and a corresponding increase in the representation of standard and difficult samples.

Following interval sampling yields notable findings. First, interval sampling efficiently mitigates the inclusion of both overly simplistic and excessively challenging samples, yielding subsets that exhibit both learnability and diversity. Fig. 3 (right) displays representative examples selected by our strategy, showcasing structural clarity coupled with contextual richness. Second, the FID of diffusion models trained on the subset \mathcal{D}_{IS} generated with increasing k initially decreases and subsequently increases. For example, as shown in Fig. 8, our results further corroborate that $k = 16$ strikes a favorable balance between sample diversity and generation quality when using a 50K data budget.



Figure 4: Visualization of samples from Random (i.e., random sampling) vs. D^2C . D^2C demonstrates a significant performance advantage over Random across all training iterations, under both a strict 0.8% (10K) and a 4% (50K) data budget, leading to a substantial acceleration in training.

3.2 Attach: Semantic and Visual Information Enhancement

To further enhance the information richness of the selected data, we introduce the *Attach* phase that augments each instance with semantic and visual information. While the *Select* phase generates a compact and informative subset, the achievable performance ceiling based solely on this phase remains limited. Consequently, we inject more comprehensive *semantic* and *visual* representations into the selected subset to further bolster our method’s generalization capability.

Dual Conditional Embedding (DC-Embedding). Existing C2I synthesis methods [11, 13] commonly rely on class embeddings trained from scratch, which often fail to effectively capture inherent semantic information (see Appendix F.1). We enrich the class embedding by incorporating text representations derived from a pre-trained text encoder (e.g., T5-encoder [35]). For each class $c \in \{1, \dots, C\}$, a descriptive prompt $P(c)$ (e.g., “a photo of a cat”) is encoded by a pre-trained text encoder f_{text} , yielding its corresponding text embedding t_c and text mask t_{mask} :

$$t_c, t_{\text{mask}} = f_{\text{text}}(P(c)), \quad (8)$$

The resulting text embedding and text mask are stored on disk as attached text information alongside the subset \mathcal{D}_{IS} generated in the preceding phase, ready for import during formal training. During the formal training, as illustrated in Fig. 5, the text embedding t_c and the text mask t_{mask} undergo a 1D convolution and are fused with a learnable class embedding e_c using a residual MLP:

$$\tilde{t}_c = \text{Conv1d}(t_c \times t_{\text{mask}}), \quad y_{\text{text}} = \text{MLP}(\tilde{t}_c) + \tilde{t}_c + e_c. \quad (9)$$

This resulting vector y_{text} then serves as a semantic conditioning token for the conditional diffusion model. Compared to using simple class embeddings alone, this formulation offers richer semantic information while retaining the learnability of class embeddings.

Visual Information Injection. While semantic information aids in distinguishing inter-class structure, it often fails to capture the intra-class variability essential for high-fidelity generation. To address this, we integrate instance-specific visual representations into the attached information. For each image $x \in \mathbb{R}^{3 \times H \times W}$, a pre-trained vision encoder f_{vis} (e.g., DINOv2 [36]) extracts patch-level semantic representations:

$$y_{\text{vis}} = f_{\text{vis}}(x) \in \mathbb{R}^{N \times d_{\text{text}}} \quad (10)$$

where N is the number of image patches and d_{text} is the feature dimension. We retain the first h (i.e., number of tokens in the diffusion transformer) tokens of y_{vis} to form a compact representation of the dominant structure: $y_{\text{vis}} = y_{\text{vis}}[:, h, :] \in \mathbb{R}^{h \times d_{\text{text}}}$. As outlined in REPA [12], this visual information provides a semantic prior for the diffusion model and thus significantly benefits data-centric efficient training. Similar to the text information y_{text} , the visual information y_{vis} is also stored on disk as attached metadata alongside the selected subset \mathcal{D}_{IS} .

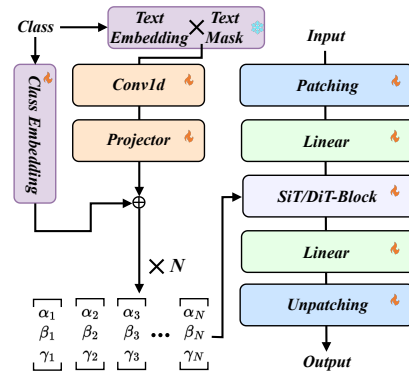


Figure 5: Overview of DC-Embedding.

Table 1: Comparison of gFID-50K across various dataset condensation methods and data budgets using DiT-L/2 and SiT-L/2 on ImageNet 256×256. We use CFG=1.5 for evaluation. D^2C surpasses other methods at all settings.

Data Budget	Iter.	DiT-L/2				SiT-L/2			
		Random	K-Center	Herding	D^2C	Random	K-Center	Herding	D^2C
0.8% (10K)	100k	35.86	50.77	40.75	4.20	4.35	14.77	22.96	3.98
0.8% (10K)	300k	4.19	13.5	22.35	4.13	4.33	13.58	22.55	3.98
4.0% (50K)	100k	36.78	69.86	32.38	14.81	31.13	61.66	29.11	11.21
4.0% (50K)	300k	11.55	38.54	22.44	5.99	14.18	39.69	22.44	5.66
8.0% (100K)	100k	41.02	71.31	36.37	22.55	36.64	66.96	32.3	15.01
8.0% (100K)	300k	11.49	37.35	15.23	6.49	12.56	39.08	16.17	5.65

Table 2: Comparison with a strict data budget 0.8% (10K) on ImageNet 512×512. We use CFG=1.5 for evaluation. D^2C surpasses random sampling at all settings. D^2C ’s performance on SiT-L/2 with 300k iterations can be found in Appendix J.

Model	Method	Iter.	gFID↓	sFID↓	IS↑	Prec.↑	Rec.↑
DiT-L/2	Random	100k	24.8	11.9	74.3	0.65	0.42
DiT-L/2	D^2C (Ours)	100k	14.8	6.9	109.2	0.63	0.52
DiT-L/2	Random	300k	17.1	12.8	130.6	0.64	0.41
DiT-L/2	D^2C (Ours)	300k	5.8	15.1	318.9	0.77	0.29
SiT-L/2	Random	100k	13.3	22.8	197.1	0.69	0.68
SiT-L/2	D^2C (Ours)	100k	9.1	14.3	261.7	0.72	0.34

3.3 D^2C Training Process

Here, we detail the training process of the diffusion model using our condensed dataset, which comprises a compact subset selected during the *Select* phase and subsequently enriched with semantic and visual information during the *Attach* phase. Our goal is to fully leverage the information existed within our condensed dataset to accelerate training without compromising performance.

We employ a conditional diffusion model \mathcal{D}_θ and, as an example, utilize the optimization objective of score-based diffusion models: predicting the added noise ϵ from the perturbed latent input \mathbf{x}_t at time step t , conditioned on the text information y_{text} and the class label y . The new denoising loss is defined as $\mathcal{L}_{\text{diff}}^{\text{new}} = \mathbb{E}_{\mathbf{x}_0 \sim q_0(\mathbf{x}), \epsilon \sim \mathcal{N}(0, \mathbf{I}), t \sim \mathcal{U}[0, 1]} [\|\epsilon - \epsilon_\theta(\mathbf{x}_t, t, y, y_{\text{text}})\|_2^2]$, where the specific injected forms of y and y_{text} can be found in Sec. 3.2. Then, to maximize the utilization of visual information, we adopt the same formulation as REPA [12], which involves aligning the encoder’s output (i.e., the decoder’s input) within the diffusion model with the visual representation $y_{\text{vis}} = \{v_i\}_{i=1}^h$. Concretely, from a designated intermediate layer of the diffusion backbone, we obtain token features $\{h_i \in \mathbb{R}^d\}_{i=1}^h$. A projection head ϕ maps these tokens from \mathbb{R}^d to $\mathbb{R}^{d_{\text{text}}}$, and we compute a semantic alignment loss:

$$\mathcal{L}_{\text{proj}} = -\frac{1}{h} \sum_{i=1}^h \left\langle \frac{\phi(h_i)}{\|\phi(h_i)\|}, \frac{v_i}{\|v_i\|} \right\rangle. \quad (11)$$

This loss encourages the model to align its encoder’s output with visual representations extracted from the visual encoder, promoting localized realism and spatial consistency [36] in generation.

Overall Training Objective. The final training loss combines the denoising objective and the semantic alignment term (with the balance weight λ is set to 0.5 by default):

$$\mathcal{L}_{\text{total}} = \mathcal{L}_{\text{diff}} + \lambda \mathbb{E}_{\mathbf{x}, \epsilon \sim \mathcal{N}(0, \mathbf{I}), t \sim \mathcal{U}[0, 1], y, y_{\text{text}}, y_{\text{vis}}} [\mathcal{L}_{\text{proj}}]. \quad (12)$$

This unified training strategy enables D^2C to effectively learn from limited yet enhanced data, offering a practical solution for efficient diffusion training under resource-constrained settings.

4 Experiments

We validate the performance of D^2C and analyze the contributions of its components through extensive experiments. In particular, we aim to answer the following questions:

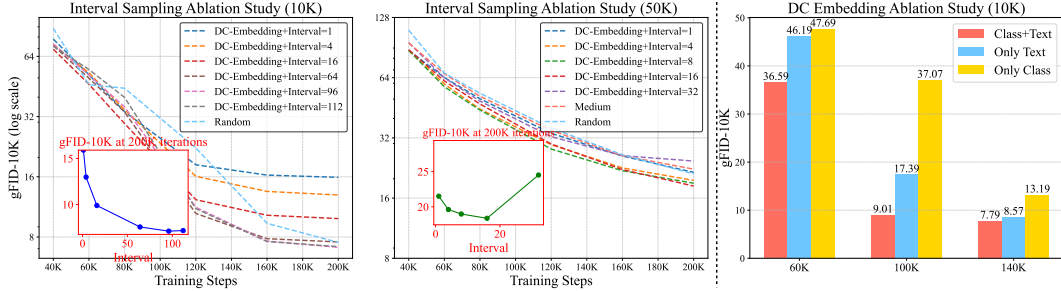


Figure 6: **Left:** Ablation studies of the interval value k in *interval sampling* at different data budgets. With a small interval value, training can experience significant acceleration during the early iterations. However, due to the limited diversity of the selected dataset, performance tends to be overtaken by random sampling in later iterations. As the interval value increases, the final gFID-10K scores initially improve and then decline, suggesting an optimal interval value exists. Notably, this optimal value is 96 for a 10K data budget and 16 for a 50K data budget, and the ratio 96/16 closely approximates the ratio of the data budgets, 50K/10K. **Right:** Ablation study of DC-Embedding under a 10K data budget. “Only Class” stands for the baseline approach of injecting class embeddings. This figure demonstrates that both the text embedding branch and the original class embedding branch (see Fig. 5) are critical for the effective training of diffusion models.

Table 3: D^2C vs. SRe²L [24] on ImageNet 256×256 with a strict data budget 0.8% (10K).

Model	Method	gFID↓	sFID↓	IS↑	Pre.↑	Rec.↑
DiT-L/2	SRe ² L	104.2	20.2	14.1	0.20	0.30
DiT-L/2	D^2C (Ours)	4.2	11.0	283.6	0.72	0.24
SiT-L/2	SRe ² L	82.3	19.8	18.1	0.27	0.19
SiT-L/2	D^2C (Ours)	3.9	10.7	289.7	0.73	0.25

- 1) Can D^2C improve training speed and reduce data usage of diffusion models? (Table 1, Figs. 1, 4)
- 2) Does D^2C generalize well across backbones, data scales, and resolutions? (Tables 1, 2, Fig. 4)
- 3) How do D^2C ’s components and hyperparameter choices affect its overall effectiveness? (Figs. 3, 6, 8)

Experiment settings. We conduct experiments on the ImageNet-1K dataset [37], using subsets of 10K, 50K, and 100K images, corresponding to 0.8%, 4%, and 8% of the full dataset, respectively. All images are center-cropped and resized to 256×256 and 512×512 resolutions using the ADM [16] preprocessing pipeline. Furthermore, we use [·]-L/2 and [·]-XL/2 architectures in both DiT [11] and SiT [13] backbones, following the standard settings outlined in Ma et al. [13]. More details on implementation and training can be found in Appendix C.

Evaluation and baselines. We train models from scratch on the collected subset and evaluate them using gFID [38], sFID, Inception Score [39], Precision (Prec.), and Recall (Rec.), adhering to standard evaluation protocols [16, 11, 13]. We compare our method against REPA [12], and various data condensation and selection baselines, including SRe²L [24], Herding, K-Center, and random sampling, using SiT and DiT architectures [13, 11]. Further details regarding evaluation metrics and baseline methods can be found in Appendix G and H.

4.1 Main Result

Training Performance and Speed. We evaluate D^2C on SiT-XL/2 using 10K and 50K data budgets, comparing its performance against REPA and a vanilla SiT model trained on the full ImageNet dataset (a 1.28M data budget), as well as random selection with 10K and 50K data budgets. As illustrated in Fig. 1 (b), our method achieves a gFID-50K of 4.23 at only 40K iterations with 10K training data and without CFG. In contrast, REPA requires 4 million steps and the vanilla SiT model needs over 7 million steps to reach comparable performance, representing an acceleration of over **100×** and **233×**, respectively. Under a 4% data budget (50K) with CFG set to 1.5, our method achieves an FID of 2.78 at 180K steps, further demonstrating significant data and compute efficiency (Fig. 1 (c)). Moreover, Fig. 4 presents a visual comparison between random selection and our D^2C at 10K and 50K data

sizes, where images are generated from the same noise and class label. Our method demonstrates superior visual quality compared to the baseline and generates higher-quality images, even during the early iterations of training.

Comparison on ImageNet 256×256. We compare D^2C with random sampling, Herding [40], K-Center [30], and SRe²L [24] under various data budgets and backbones. As illustrated in Table 1, D^2C consistently achieves the lowest FID across all settings. For instance, using only 0.8% of the data and 100K iterations with early stopping, our method achieves a gFID-50K of 4.20 on DiT-L/2 and 3.98 on SiT. These results demonstrate the superiority of our approach over existing methods. Notably, SRe²L, which performs well in classification task, fails on this generative task (see Table 3) due to its focus on category-discriminative features. Similarly, geometry-based methods like Herding and K-Center, along with random sampling, prove inadequate for achieving efficient and high-performing training of diffusion models.

Comparison on ImageNet 512×512. As shown in Table 2, D^2C achieves a gFID of 5.8 on DiT-L/2, a significant improvement over the 17.1 achieved by random sampling at 300k iterations under the ImageNet 512×512 settings. On SiT-L/2, similar improvements are observed. These results demonstrate that D^2C generalizes well to higher resolutions.

4.2 Ablation Study

Ablation on Select Phase. We investigate the impact of the interval value k in the *Select* phase, as shown in Fig. 6 (Left) and Fig. 7. Using a small value accelerates early training by prioritizing min-loss samples, which are simpler and easier to learn. However, the limited diversity of such samples leads to degraded performance in later stages, eventually being overtaken by settings with moderate interval values. In contrast, large intervals or random selection introduce excessive max-loss or uncured samples, destabilizing training (Fig. 3). As k increases, we observe that gFID-10K first decreases and then worsens, revealing an optimal trade-off between diversity and learnability. Empirically, the best results are achieved with an interval of 96 for the 10K budget and 16 for 50K, approximately following the ratio of data budgets (50K/10K).

Ablation on Attach Phase. We conduct ablation studies on the *Attach* phase from two perspectives. First, as shown in Fig. 6 (Right), we examine the effectiveness of dual conditional embedding under a 10K data budget. Using only class or text embedding results in degraded performance compared to their combination, indicating the necessity of both components to capture category semantics and text embeddings. Notably, text embedding alone performs better than class embedding, suggesting that textual descriptions provide richer semantic information for generative tasks. Second, as shown in Table 4, we analyze the impact of the semantic and visual information injection modules. The gFID-10K increases to 37.07 when both branches are removed and to 9.01 when only the visual injection module is excluded. Notably, the combination of both modules yields the best FID of 7.62. These results underscore the crucial role of injecting both semantic and visual information in accelerating diffusion model training.

5 Conclusion

In this paper, we introduce D^2C , the first dataset condensation framework that can significantly accelerate diffusion model training for the generative task. Our pipeline comprises two key phases: *Select* and *Attach*. In the *Select* phase, we leverage diffusion difficulty score and interval sampling to obtain a subset that is both compact and diverse. Subsequently, in the *Attach* phase, we augment this

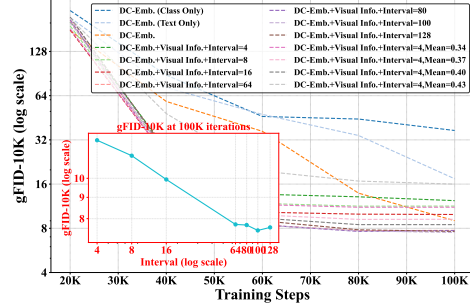


Figure 7: Ablation studies of interval sampling and DC-Embedding. “Mean=N” denotes the selection of a subset of samples where the average diffusion loss is closest to the value N.

Model	Semantic Info.	Visual Info.	gFID-10K↓
DiT-L/2	✗	✗	37.07
DiT-L/2	✓	✗	9.01
DiT-L/2	✓	✓	7.62

Table 4: Ablation on semantic and visual information in the Attach phase.

subset with critical semantic and visual information, leading to a dramatic improvement in the training acceleration ratio and enhanced performance robustness. While there are still some limitations (refer to Appendix A), our D^2C as the pioneering work in this novel approach still achieved impressively $100 \sim 233\times$ training acceleration over the baselines. We believe that our work will offer novel inspirations and motivate more research on this promising field in the future.

Broader Impact

We introduce D^2C , a method engineered to decrease training overhead while minimizing performance degradation. The dataset employed for training D^2C was ImageNet-1K, which adheres to ethical guidelines. Moreover, we prioritize the responsible and ethical deployment of this technology, aiming to maximize its societal benefits while proactively addressing and mitigating any potential risks.

References

- [1] Yang Song, Jascha Sohl-Dickstein, Diederik P Kingma, Abhishek Kumar, Stefano Ermon, and Ben Poole. Score-based generative modeling through stochastic differential equations. In *International Conference on Learning Representations*, kigali, rwanda, May. 2023. OpenReview.net.
- [2] Jiaming Song, Chenlin Meng, and Stefano Ermon. Denoising diffusion implicit models. In *International Conference on Learning Representations*, kigali, rwanda, May. 2023. OpenReview.net.
- [3] Jonathan Ho, Ajay Jain, and Pieter Abbeel. Denoising diffusion probabilistic models. In *Neural Information Processing Systems*, pages 6840–6851, Virtual Event, Dec. 2020. NeurIPS.
- [4] Jonathan Ho and Tim Salimans. Classifier-free diffusion guidance. In *Neural Information Processing Systems Workshop*, Virtual Event, Dec. 2021. NeurIPS.
- [5] Xingchao Liu, Chengyue Gong, and Qiang Liu. Flow straight and fast: Learning to generate and transfer data with rectified flow. *arXiv preprint arXiv:2209.03003*, 2022.
- [6] Stability.ai. Introducing stable diffusion 3.5. <https://stability.ai/news/introducing-stable-diffusion-3-5>, 2024.
- [7] Patrick Esser, Sumith Kulal, Andreas Blattmann, Rahim Entezari, Jonas Müller, Harry Saini, Yam Levi, Dominik Lorenz, Axel Sauer, Frederic Boesel, et al. Scaling rectified flow transformers for high-resolution image synthesis. In *Forty-first International Conference on Machine Learning*, 2024.
- [8] Tero Karras, Miika Aittala, Timo Aila, and Samuli Laine. Elucidating the design space of diffusion-based generative models. *Advances in neural information processing systems*, 35: 26565–26577, 2022.
- [9] Dustin Podell, Zion English, Kyle Lacey, Andreas Blattmann, Tim Dockhorn, Jonas Müller, Joe Penna, and Robin Rombach. Sdxl: Improving latent diffusion models for high-resolution image synthesis. In *The Twelfth International Conference on Learning Representations*.
- [10] Yuwei Guo, Ceyuan Yang, Anyi Rao, Zhengyang Liang, Yaohui Wang, Yu Qiao, Maneesh Agrawala, Dahua Lin, and Bo Dai. Animatediff: Animate your personalized text-to-image diffusion models without specific tuning. *arXiv preprint arXiv:2307.04725*, 2023.
- [11] William Peebles and Saining Xie. Scalable diffusion models with transformers. In *Proceedings of the IEEE/CVF International Conference on Computer Vision*, pages 4195–4205, 2023.
- [12] Sihyun Yu, Sangkyung Kwak, Huiwon Jang, Jongheon Jeong, Jonathan Huang, Jinwoo Shin, and Saining Xie. Representation alignment for generation: Training diffusion transformers is easier than you think. In *International Conference on Learning Representations*, 2025.
- [13] Nanye Ma, Mark Goldstein, Michael S Albergo, Nicholas M Boffi, Eric Vanden-Eijnden, and Saining Xie. Sit: Exploring flow and diffusion-based generative models with scalable interpolant transformers. In *European Conference on Computer Vision*, pages 23–40. Springer, 2024.
- [14] Xinglin Li, Jiajing Chen, Jinhui Ouyang, Hanhui Deng, Senem Velipasalar, and Di Wu. Tothepoint: Efficient contrastive learning of 3d point clouds via recycling. In *Computer Vision and Pattern Recognition*, pages 21781–21790, Vancouver, BC, Canada, June 2023. IEEE.
- [15] Justin Cui, Ruochen Wang, Si Si, and Cho-Jui Hsieh. DC-BENCH: dataset condensation benchmark. In *Neural Information Processing Systems*, New Orleans, LA, USA, Nov. 2022. NeurIPS.

- [16] Prafulla Dhariwal and Alexander Nichol. Diffusion models beat gans on image synthesis. In *Neural Information Processing Systems*, volume 34, pages 8780–8794, Virtual Event, Dec. 2021. NeurIPS.
- [17] Daniel Bolya and Judy Hoffman. Token merging for fast stable diffusion. In *Proceedings of the IEEE/CVF conference on computer vision and pattern recognition*, pages 4599–4603, 2023.
- [18] Cheng Lu, Yuhao Zhou, Fan Bao, Jianfei Chen, Chongxuan Li, and Jun Zhu. Dpm-solver: A fast ode solver for diffusion probabilistic model sampling in around 10 steps. In *Neural Information Processing Systems*, New Orleans, LA, USA, Nov.-Dec. 2022. NeurIPS.
- [19] Kaiwen Zheng, Cheng Lu, Jianfei Chen, and Jun Zhu. Dpm-solver-v3: Improved diffusion ode solver with empirical model statistics. *Advances in Neural Information Processing Systems*, 36: 55502–55542, 2023.
- [20] Cheng Lu, Yuhao Zhou, Fan Bao, Jianfei Chen, and Chongxuan Li. Dpm-solver++: Fast solver for guided sampling of diffusion probabilistic models. *arXiv preprint arXiv:2211.01095*, 2022.
- [21] Zhendong Wang, Yifan Jiang, Huangjie Zheng, Peihao Wang, Pengcheng He, Zhangyang Wang, Weizhu Chen, Mingyuan Zhou, et al. Patch diffusion: Faster and more data-efficient training of diffusion models. *Advances in neural information processing systems*, 36:72137–72154, 2023.
- [22] Tongzhou Wang, Jun-Yan Zhu, Antonio Torralba, and Alexei A Efros. Dataset distillation. *arXiv preprint arXiv:1811.10959*, 2018.
- [23] Kai Wang, Bo Zhao, Xiangyu Peng, Zheng Zhu, Shuo Yang, Shuo Wang, Guan Huang, Hakan Bilen, Xinchao Wang, and Yang You. Cafe: Learning to condense dataset by aligning features. In *Computer Vision and Pattern Recognition*, pages 12196–12205, New Orleans, LA, USA, Jun. 2022. IEEE.
- [24] Zeyuan Yin, Eric P. Xing, and Zhiqiang Shen. Squeeze, recover and relabel: Dataset condensation at imagenet scale from A new perspective. In *Neural Information Processing Systems*. NeurIPS, 2023.
- [25] Shitong Shao, Zeyuan Yin, Xindong Zhang, and Zhiqiang Shen. Generalized large-scale data condensation via various backbone and statistical matching. *arXiv preprint arXiv:2311.17950*, 2023.
- [26] Shuo Yang, Zeke Xie, Hanyu Peng, Min Xu, Mingming Sun, and Ping Li. Dataset pruning: Reducing training data by examining generalization influence. In *The Eleventh International Conference on Learning Representations*, 2023.
- [27] Peng Sun, Bei Shi, Daiwei Yu, and Tao Lin. On the diversity and realism of distilled dataset: An efficient dataset distillation paradigm. In *Computer Vision and Pattern Recognition*. IEEE, 2024.
- [28] Laura Manduchi, Kushagra Pandey, Clara Meister, Robert Bamler, Ryan Cotterell, Sina Däubener, Sophie Fellenz, Asja Fischer, Thomas Gärtner, Matthias Kirchler, et al. On the challenges and opportunities in generative ai. *arXiv preprint arXiv:2403.00025*, 2024.
- [29] Tianhong Li, Dina Katabi, and Kaiming He. Return of unconditional generation: A self-supervised representation generation method. *Advances in Neural Information Processing Systems*, 37:125441–125468, 2024.
- [30] Matthew Jones, Huy Nguyen, and Thy Nguyen. Fair k-centers via maximum matching. In *International conference on machine learning*, pages 4940–4949. PMLR, 2020.
- [31] Yutian Chen and Max Welling. Parametric herding. In *Proceedings of the Thirteenth International Conference on Artificial Intelligence and Statistics*, pages 97–104. JMLR Workshop and Conference Proceedings, 2010.
- [32] Shitong Shao, Zikai Zhou, Huanran Chen, and Zhiqiang Shen. Elucidating the design space of dataset condensation. *arXiv preprint arXiv:2404.13733*, 2024.

- [33] George Cazenavette, Tongzhou Wang, Antonio Torralba, Alexei A. Efros, and Jun-Yan Zhu. Dataset distillation by matching training trajectories. In *Computer Vision and Pattern Recognition*, New Orleans, LA, USA, Jun. 2022. IEEE.
- [34] Alexander C Li, Mihir Prabhudesai, Shivam Duggal, Ellis Brown, and Deepak Pathak. Your diffusion model is secretly a zero-shot classifier. In *Proceedings of the IEEE/CVF International Conference on Computer Vision*, pages 2206–2217, 2023.
- [35] Jianmo Ni, Gustavo Hernandez Abrego, Noah Constant, Ji Ma, Keith B Hall, Daniel Cer, and Yinfei Yang. Sentence-t5: Scalable sentence encoders from pre-trained text-to-text models. *arXiv preprint arXiv:2108.08877*, 2021.
- [36] Maxime Oquab, Timothée Darcet, Théo Moutakanni, Huy Vo, Marc Szafraniec, Vasil Khalidov, Pierre Fernandez, Daniel Haziza, Francisco Massa, Alaaeldin El-Nouby, et al. Dinov2: Learning robust visual features without supervision. *arXiv preprint arXiv:2304.07193*, 2023.
- [37] Olga Russakovsky, Jia Deng, Hao Su, Jonathan Krause, Sanjeev Satheesh, Sean Ma, Zhiheng Huang, Andrej Karpathy, Aditya Khosla, Michael Bernstein, et al. Imagenet large scale visual recognition challenge. *International Journal of Computer Vision*, 115(3):211–252, 2015.
- [38] Martin Heusel, Hubert Ramsauer, Thomas Unterthiner, Bernhard Nessler, and Sepp Hochreiter. Gans trained by a two time-scale update rule converge to a local nash equilibrium. In *Neural Information Processing Systems*, volume 30, Long Beach Convention Center, Long Beach, Dec. 2017. NeurIPS.
- [39] Tim Salimans, Ian Goodfellow, Wojciech Zaremba, Vicki Cheung, Alec Radford, and Xi Chen. Improved techniques for training gans. In *Neural Information Processing Systems*, volume 29, Centre Convencions Internacional Barcelona, Barcelona SPAIN, Dec. 2016. NeurIPS.
- [40] Haoxin Chen, Menghan Xia, Yingqing He, Yong Zhang, Xiaodong Cun, Shaoshu Yang, Jinbo Xing, Yaofang Liu, Qifeng Chen, Xintao Wang, et al. Videocrafter1: Open diffusion models for high-quality video generation. *arXiv preprint arXiv:2310.19512*, 2023.
- [41] Alexey Dosovitskiy, Lucas Beyer, Alexander Kolesnikov, Dirk Weissenborn, Xiaohua Zhai, Thomas Unterthiner, Mostafa Dehghani, Matthias Minderer, Georg Heigold, Sylvain Gelly, et al. An image is worth 16x16 words: Transformers for image recognition at scale. In *International Conference on Learning Representations*, Event Virtual, May 2020. OpenReview.net.
- [42] Diederik P Kingma. Auto-encoding variational bayes. *arXiv preprint arXiv:1312.6114*, 2013.
- [43] Alec Radford, Jong Wook Kim, Chris Hallacy, Aditya Ramesh, Gabriel Goh, Sandhini Agarwal, Girish Sastry, Amanda Askell, Pamela Mishkin, Jack Clark, Gretchen Krueger, and Ilya Sutskever. Learning transferable visual models from natural language supervision, 2021.
- [44] Christian Szegedy, Vincent Vanhoucke, Sergey Ioffe, Jon Shlens, and Zbigniew Wojna. Re-thinking the inception architecture for computer vision. In *Proceedings of the IEEE conference on computer vision and pattern recognition*, pages 2818–2826, 2016.
- [45] Charlie Nash, Jacob Menick, Sander Dieleman, and Peter W Battaglia. Generating images with sparse representations. *arXiv preprint arXiv:2103.03841*, 2021.
- [46] Tuomas Kynkäänniemi, Tero Karras, Samuli Laine, Jaakko Lehtinen, and Timo Aila. Improved precision and recall metric for assessing generative models. *Advances in neural information processing systems*, 32, 2019.
- [47] Kaiming He, Xinlei Chen, Saining Xie, Yanghao Li, Piotr Dollár, and Ross Girshick. Masked autoencoders are scalable vision learners. In *Proceedings of the IEEE/CVF conference on computer vision and pattern recognition*, pages 16000–16009, 2022.
- [48] Kaiming He, Haoqi Fan, Yuxin Wu, Saining Xie, and Ross Girshick. Momentum contrast for unsupervised visual representation learning. In *Proceedings of the IEEE/CVF conference on computer vision and pattern recognition*, pages 9729–9738, 2020.

Appendix

A Limitation

This work primarily focuses on accelerating and improving the training process of diffusion models. While our approach demonstrates promising results in the early stage, the final performance upon convergence does not yet fully match baseline benchmarks. It is important to unleash the potential of our algorithm, such as fine-tuning the vision and text encoders to better align noise latent features with the integrated visual information, thereby reducing existing discrepancies. Additionally, although the current study centers on image generation tasks, extending our method to other domains, such as 3D generation and video synthesis, represents a promising direction for future exploration.

B Additional Descriptions of Diffusion Models

This section presents the preliminaries of the diffusion model. For simplicity, we introduce the standard denoising diffusion probabilistic model (DDPM), where the forward process gradually corrupts the input with noise and the reverse process restores the target data distribution. We also summarize the architectural details in B.2.

B.1 Denoising Diffusion Probabilistic Model (DDPM)

The DDPM framework models data generation via a discrete-time Markov chain that progressively adds Gaussian noise to a data sample $x_0 \sim p(x)$. The forward process is defined as:

$$q(x_t | x_{t-1}) = \mathcal{N}(x_t; \sqrt{1 - \beta_t}x_{t-1}, \beta_t \mathbf{I}), \quad (13)$$

where $\beta_t \in (0, 1)$ are predefined variance schedule parameters controlling the noise level at each time step $t \in [1, 2, \dots, T]$, and \mathbf{I} is the identity matrix.

For simplicity, we define $\alpha_t = 1 - \beta_t$, and denote the cumulative product $\bar{\alpha}_t = \prod_{i=1}^t \alpha_i$. The reverse process, which is learned by the model θ , can be defined as:

$$p_\theta(x_{t-1} | x_t) = \mathcal{N}\left(x_{t-1}; \frac{1}{\sqrt{\alpha_t}} \left(x_t - \frac{\beta_t}{\sqrt{1 - \bar{\alpha}_t}} \epsilon_\theta(x_t, t)\right), \Sigma_\theta(x_t, t)\right), \quad (14)$$

where $\epsilon_\theta(x_t, t)$ denotes the predicted noise from a neural network. The covariance $\Sigma_\theta(x_t, t)$ is typically set to $\sigma_t^2 \mathbf{I}$, where σ_t^2 can be either fixed ($\sigma_t^2 = \beta_t$) or learned through interpolation $\sigma_t^2 = (1 - \bar{\alpha}_{t-1})/(1 - \bar{\alpha}_t)\beta_t$.

A simplified training objective minimizes the prediction error between true and estimated noise:

$$\mathcal{L}_{\text{simple}} = \mathbb{E}_{x_0, \epsilon, t} [\|\epsilon - \epsilon_\theta(\sqrt{\bar{\alpha}_t}x_0 + \sqrt{1 - \bar{\alpha}_t}\epsilon, t)\|^2] \quad (15)$$

In addition to the simple objective, improved variants include learning the reverse variance $\Sigma_\theta(x_t, t)$ jointly with the mean, which leads to a variational bound loss of the form:

$$\mathcal{L}_{\text{vib}} = \exp\left(v \log \beta_t + (1 - v) \log \tilde{\beta}_t\right) \quad (16)$$

Here, v is an element-wise weight across model output dimensions. When T is sufficiently large and the noise schedule is carefully chosen, the terminal distribution $p(x_T)$ approximates an isotropic Gaussian. Sampling is then performed by iteratively applying the learned reverse process to recover the data sample from pure noise.

B.2 Diffusion Transformer Architecture

Our model implementation closely follows the design of DiT [11] and SiT [13], which extend the vision transformer (ViT) architecture [41] to generative modeling. An input image is first split into patches, reshaped into a 1D sequence of length N , and then processed through transformer layers. To

reduce spatial resolution and computational cost, we follow prior work [11, 13] and encode the image into a latent tensor $z = E(x)$ using a pretrained encoder E from the stable diffusion VAE [42].

In contrast to the standard ViT, our transformer blocks include time-aware adaptive normalization layers known as AdaIN-zero. These layers scale and shift the hidden state in each attention block according to the diffusion timestep and conditioning signals. During training, we also add an auxiliary multilayer perceptron (MLP) head that maps the hidden state to a semantic target representation space, such as DINOv2 [36] or CLIP features [43]. This head is used only for training-time supervision in our alignment loss and does not affect sampling or inference.

C Hyperparameters and Implementation Details

Select Phase Settings. In the *Select* phase, we adopt a pre-trained DiT-XL/2 model [11] as the scoring network and use the diffusion loss (mean squared error) as the scoring metric. To construct subsets of different sizes, we apply interval sampling with $k = 96$ for the 10K subset, $k = 16$ for the 50K subset, and $k = 10$ for the 100K subset. Each subset is constructed in a class-wise manner, selecting 10, 50, and 100 samples per class respectively.

Attach Phase Settings. In the *Attach* phase, we implement dual conditional embeddings. For textual conditioning, we use a T5 encoder [35] with captions truncated to 16 tokens, producing embeddings of dimension 2048. For visual conditioning, we adopt DINOv2-B [36] as the visual encoder. The number of visual tokens h is set to 256, and each token has a feature dimension of 768.

Training Settings. In the *Training* phase, we use the Adam optimizer with a fixed learning rate of $1e-4$ and $(\beta_1, \beta_2) = (0.9, 0.999)$, without applying weight decay. We employ mixed-precision (fp16) training with gradient clipping. Latent representations are pre-computed using the stable diffusion VAE [42], and decoded via its native decoder. All experiments are conducted on either 8 NVIDIA A800 80GB GPUs or 8 NVIDIA RTX 4090 24GB GPUs. We use a batch size of 256 with a 256×256 resolution in Figure 1, and a 512×512 resolution in Table 2. All other experiments use a batch size of 128 and a default image resolution of 256×256 .

D Framework Design and Implementation

The design of D²C aims to construct compact yet effective training subsets for diffusion models under strict data budgets. It is built on two complementary intuitions: (1) not all training samples contribute equally—some are easier to learn and more informative; and (2) generative training benefits from semantically enriched conditioning. These insights motivate the Select phase, which ranks samples by diffusion-estimated difficulty, using a pre-trained class-conditional diffusion model to compute a scoring function over training examples. The Attach phase then injects textual and visual priors. While empirical in nature, the framework draws from ideas in curriculum learning, semantic conditioning, and representation alignment. The full process is summarized in Algorithm 1.

Algorithm 1 D²C: Diffusion Dataset Condensation

Require: Full dataset $\mathcal{D} = \{(x_i, c_i)\}_{i=1}^N$, interval k , text encoder f_{text} , visual encoder f_{vis}
// Each x_i is an image, and $c_i \in \{1, \dots, C\}$ is the class label.

- 1: **// Phase 1: Select**
 - 2: Compute difficulty score s_{diff} for all $(x_i, c_i) \in \mathcal{D}$
 - 3: For each class c , sort $\mathcal{D}_c = \{x_i \mid c_i = c\}$ by s_{diff} descending
 - 4: Select every k -th sample (Interval Sampling) in sorted \mathcal{D}_c to form $\mathcal{D}_{\text{select}}$
 - 5: **// Phase 2: Attach**
 - 6: **for** each $(x, c) \in \mathcal{D}_{\text{select}}$ **do**
 - 7: Generate class prompt $P(c)$ (e.g., “a photo of a label”)
 - 8: Extract text embedding: $(t_c, t_{\text{mask}}) \leftarrow f_{\text{text}}(P(c))$
 - 9: Extract visual feature: $y_{\text{vis}} \leftarrow f_{\text{vis}}(x)$
 - 10: Store triplet $(x, c, t_c, t_{\text{mask}}, y_{\text{vis}})$ into $\tilde{\mathcal{D}}$
 - 11: **end for**
 - 12: **Return** enriched dataset $\tilde{\mathcal{D}}$ for diffusion model training
-

E More Discussions about Select

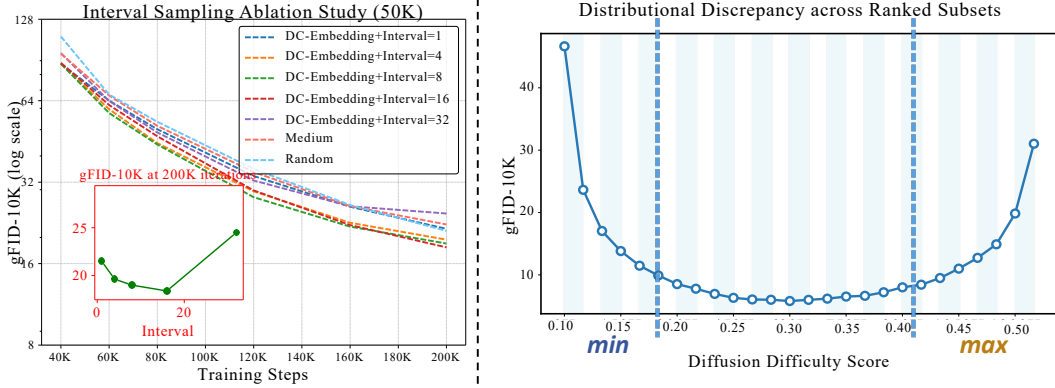


Figure 8: **Left:** gFID-10K across training steps under different interval values k for a 50K data budget. Moderate intervals (e.g., $k = 16$) achieve superior performance by balancing learnability and diversity. **Right:** Distributional discrepancy (gFID-10K) between ranked training subsets and the validation set. Both extremely low and high diffusion difficulty scores lead to higher FID, while mid-range segments show better alignment.

While Section 4.2 has covered a detailed ablation study on the choice of interval k in *Select* phase, we provide additional insights into how diffusion difficulty scores relate to distributional coverage.

The right panel in Fig. 8 presents the gFID-10K scores of subsets sampled from different portions of the difficulty-ranked dataset. We partition the training set into consecutive 10K segments ordered by the diffusion difficulty score (e.g., the first 10K samples with lowest scores as “Min”, followed by 10–20K, 20–30K, and so on), and measure each segment’s discrepancy from the full validation distribution using gFiD. Interestingly, we observe a clear U-shaped curve: subsets consisting of extremely low or high difficulty samples exhibit significantly worse distributional alignment, while those centered around moderate difficulty levels show substantially lower FID scores. This result aligns well with our hypothesis that very easy samples (e.g., simple textures, clean backgrounds) and extremely hard samples (e.g., ambiguous, noisy structures) both fail to reflect the global data distribution.

These observations provide an empirical justification for our interval sampling strategy. Specifically, under a 50K dataset budget with $k = 16$, each class contributes samples selected at regular intervals from its difficulty-sorted list. Given that each class typically contains around 1,200 images, this strategy naturally samples from approximately the first 800 positions in the ranked list. As a result, the selected data span both the easy and moderately difficult regions, while avoiding the extremes at both ends. This balanced coverage across the difficulty spectrum promotes better generalization and faster convergence, as evidenced by the results in Fig. 8 (Left) and discussed in Section 4.2. In this way, our strategy yields a compact yet effective dataset that enables the model to converge rapidly while maintaining strong generation quality.

F More Discussion about Attach

F.1 Dual Conditional Embedding

Most diffusion models condition on class identifiers represented as integer IDs or one-hot vectors, which are mapped to class embeddings trained from scratch. This ignores semantic relationships between categories, resulting in unstructured embeddings as shown in Figure 9 (Left). In contrast, text embeddings derived from class-specific prompts (e.g., “a photo of a dog”) via a pre-trained language encoder naturally encode semantic priors and cluster related classes (Figure 9, Right). We propose a dual conditional embedding that fuses the text embedding with a learnable class embedding (i.e., a traditional class token trained from scratch), as defined in Eq. 8–9. This hybrid strategy combines semantic structure with symbolic distinctiveness, and leads to significantly improved generation quality. As shown in Figure 6 (Right), using both branches achieves lower FID than using either one alone.

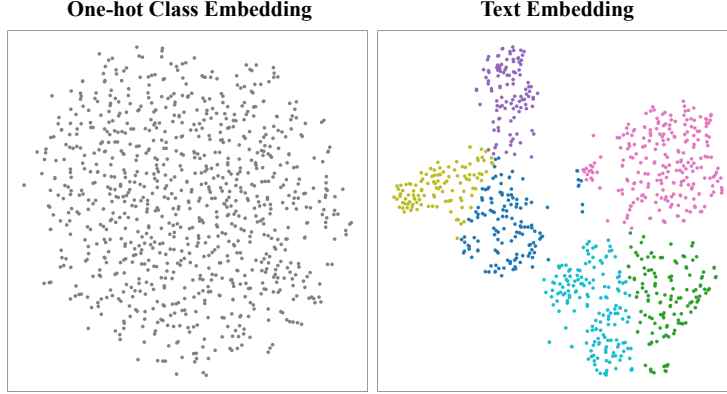


Figure 9: t-SNE visualization of class embeddings. Each point represents a class in the dataset. **Left:** One-hot class embeddings show no semantic structure. **Right:** Text embeddings naturally cluster semantically related classes.

F.2 Visual Information Injection

Recent studies[12] have shown that relying solely on diffusion models to learn meaningful representations from scratch often results in suboptimal semantic features. In contrast, injecting high-quality visual priors, especially those derived from strong self-supervised encoders like DINOv2[36], can significantly improve both training efficiency and generation quality. In our case, we incorporate a frozen visual encoder (DINOv2) to provide external patch-level visual features during training. These external features serve as semantically rich anchors, particularly beneficial at early layers, allowing the model to focus on generation-specific details in later stages. Empirically, we observe that such visual supervision leads to better feature alignment and faster convergence under limited data budgets, as evidenced in Table 1, 2, and 4.

G Evaluation Details

We adopt several widely used metrics to evaluate generation quality and diversity:

- **gFID** [38] computes the Fréchet distance between the feature distributions of real and generated images. Features are extracted using the Inception-v3 network [44].
- **sFID** [45] extends FID by leveraging intermediate spatial features from the Inception-v3 model to better capture spatial structure and style in generated images.
- **IS** [39] evaluates both the quality and diversity of generated samples by computing the KL-divergence between the conditional label distribution and the marginal distribution over predicted classes, using softmax-normalized logits.
- **Precision and Recall** [46] respectively measure sample realism and diversity, quantifying how well generated samples cover the data manifold and vice versa.

H Baseline Setting

We evaluate our method against two categories of baselines:

Diffusion models trained on selected or condensed subsets. These include SiT and DiT backbones trained from scratch on 10K, 50K, and 100K subsets obtained via the following strategies:

- **Random Sampling.** A naive baseline that randomly selects a fixed number of real samples without any guidance.
- **Herdning** [31]. A geometry-based method that selects samples to approximate the global feature mean, ensuring representative coverage.
- **K-Center** [30]. A diversity-focused algorithm that iteratively selects samples maximizing the minimum distance from the selected set, promoting broad coverage of the feature space.

- **SRe²L** [24]. A dataset condensation method that synthesizes class-conditional data through a multi-stage pipeline. Originally proposed for classification tasks, we adapt it to the diffusion setting by applying class-wise condensation to real images and training a diffusion model on the resulting synthetic subset. Visualizations of the synthesized samples and corresponding training results are provided in Appendix I.

Diffusion models trained on the full dataset. These baselines are trained with access to the entire training set, without data reduction:

- **SiT** [13]. A transformer-based diffusion model that reformulates denoising as continuous stochastic interpolation, enabling faster training and improved efficiency under full-data settings.
- **REPA** [12]. A model-side regularization method that aligns intermediate features of diffusion transformers with patch-wise representations from strong pretrained visual encoders (e.g., DINOv2-B [36], MAE [47], MoCov3 [48]) using a contrastive loss. It retains the full dataset and improves convergence and generation quality via early-layer representation guidance.

I Visualization of SRe²L in Generative Tasks



Figure 10: **Top:** images synthesized directly by SRe²L, a popular dataset condensation method originally designed for discriminative tasks. **Bottom:** images generated by a diffusion model trained on the SRe²L dataset. As exemplified by SRe²L, such methods often struggle in generative settings—producing blurry, low-fidelity outputs that are poorly aligned with the true data distribution.

J ImageNet 512×512 Experiment

As shown in Table 5, D^2C consistently outperforms random sampling under a strict 10K (0.8%) data budget across both DiT-L/2 and SiT-L/2 backbones. At 300k iterations, our method achieves a gFID of 5.8 on DiT-L/2 and 4.22 on SiT-L/2, showing strong improvements. Visual samples in Figure 11 further confirm the high fidelity and diversity of generations at 512×512 resolution, demonstrating that D^2C generalizes effectively to high-resolution settings.

Table 5: Comparison with a data budget 0.8% (10K) on ImageNet 512×512 (CFG=1.5).

Model	Method	Iter.	gFID↓	sFID↓	IS↑	Prec.↑	Rec.↑
DiT-L/2	Random	100k	24.8	11.9	74.3	0.65	0.42
DiT-L/2	D^2C (Ours)	100k	14.8	6.9	109.2	0.63	0.52
DiT-L/2	Random	300k	17.1	12.8	130.6	0.64	0.41
DiT-L/2	D^2C (Ours)	300k	5.8	15.1	318.9	0.77	0.29
SiT-L/2	Random	100k	13.3	22.8	197.1	0.69	0.68
SiT-L/2	D^2C (Ours)	100k	9.1	14.3	261.7	0.72	0.34
SiT-L/2	Random	300k	5.0	13.6	316.9	0.76	0.27
SiT-L/2	D^2C (Ours)	300k	4.22	11.6	289.7	0.79	0.24



Figure 11: Generated samples on ImageNet 512×512 from SiT-L/2 trained with D^2C using a 10K dataset (CFG=1.5).

K Visualization



Figure 12: Generated samples of SiT-L/2 trained with D^2C using a 50K dataset (CFG=1.5). Class label = "macaw"(88)



Figure 13: Generated samples of SiT-L/2 trained with D^2C using a 50K dataset (CFG=1.5). Class label = "arctic wolf"(270)

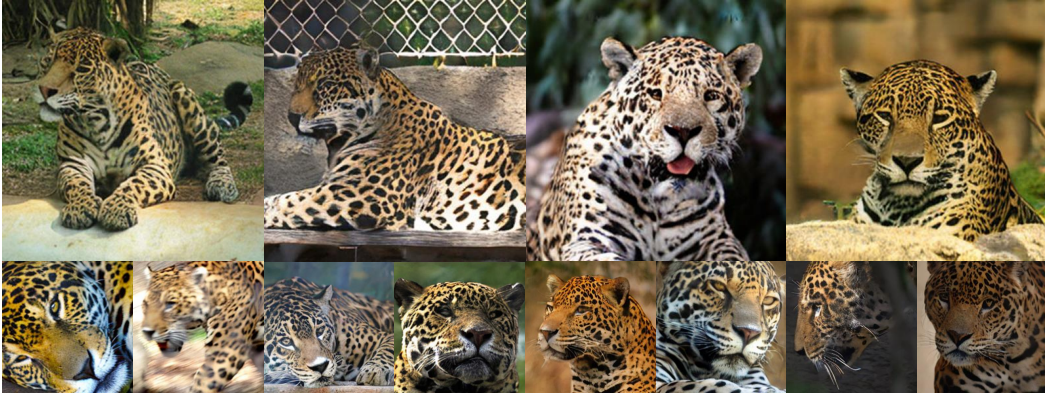


Figure 14: Generated samples of SiT-L/2 trained with D^2C using a 50K dataset (CFG=1.5). Class label = "jaguar"(290)



Figure 15: Generated samples of SiT-L/2 trained with D^2C using a 50K dataset (CFG=1.5). Class label = "otter"(360)



Figure 16: Generated samples of SiT-L/2 trained with D^2C using a 50K dataset (CFG=1.5). Class label = "lesser panda"(387)



Figure 17: Generated samples of SiT-L/2 trained with D^2C using a 50K dataset (CFG=1.5). Class label = "panda"(388)



Figure 18: Generated samples of SiT-L/2 trained with D^2C using a 50K dataset (CFG=1.5). Class label = "fire truck"(555)



Figure 19: Generated samples of SiT-L/2 trained with D^2C using a 50K dataset (CFG=1.5). Class label = "cheeseburger"(933)

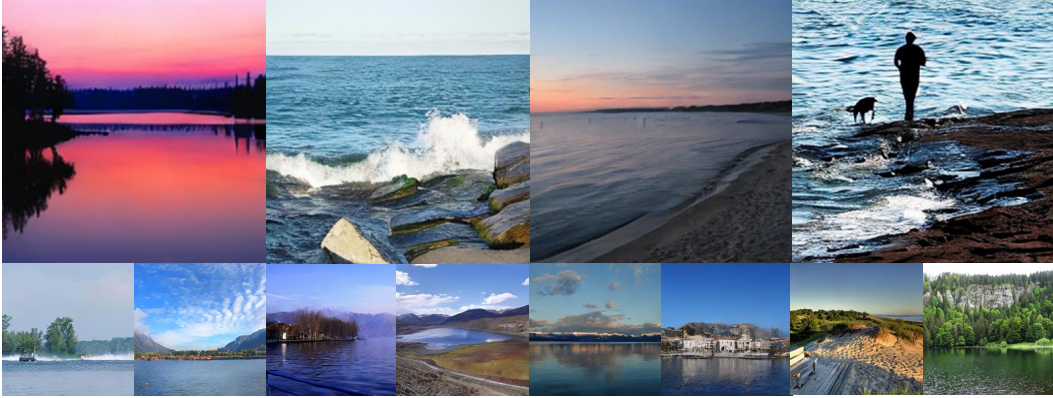


Figure 20: Generated samples of SiT-L/2 trained with D^2C using a 50K dataset (CFG=1.5). Class label = "lake shore"(975)



Figure 21: Generated samples of SiT-L/2 trained with D^2C using a 50K dataset (CFG=1.5). Class label = "volcano"(980)